REVIEW ARTICLE
https://doi.org/10.1038/s41565-018-0320-y

nature nanotechnology

Applications of nanolasers

Ren-Min Ma[1,2*] and Rupert F. Oulton[3]

Nanolasers generate coherent light at the nanoscale. In the past decade, they have attracted intense interest, because they are more compact, faster and more power-efficient than conventional lasers. Thanks to these capabilities, nanolasers are now an emergent tool for a variety of practical applications. In this Review, we explain the intrinsic merits of nanolasers and assess recent progress on their applications, particularly for optical interconnects, near-field spectroscopy and sensing, optical probing for biological systems and far-field beam synthesis through near-field eigenmode engineering. We highlight the scientific and engineering challenges that remain for forging nanolasers into powerful tools for nanoscience and nanotechnology.

It is difficult to overstate the impact of lasers on our society. Since Theodore Maiman's first demonstration in 1960[1], lasers have become a pervasive technology that enables a range of consumer technologies and data communications systems, as well as driving fundamental research in virtually every field. Lasers generate light with strong spectral and temporal localization, and large laser facilities with increasingly powerful devices are being built to achieve nuclear fusion[2]. At the other extreme, creating lasers with increasingly smaller physical sizes has been a research goal since the beginning. Initially, the main drive was technological, aiming at more compact size and lower power consumption; but when the size of lasers reached wavelength scales in the 1990s, another strong reason became obvious: light interacts differently with matter at the nanoscale. Fundamental knowledge soon translated into unique applications, such as ultra-dense data storage, nanolithography, sensing, super-resolution imaging and optical interconnects[3–6].

Pioneering efforts in nanolasers date back to the turn of the century with the demonstration of microdisk lasers[7], photonic crystal lasers[8] and nanowire lasers[9]. Microdisk lasers use the whispering gallery mode for efficient cavity feedback. Photonic crystal lasers confine an optical cavity mode to a wavelength scale by exploiting the optical bandgap of photonic crystals in otherwise fairly large periodically etched dielectric nanostructure arrays. Semiconductor nanowires also have excellent optical field confinement but, in addition, exploit nanoscale dimensions to manage crystal strain, which eliminates the restrictions of conventional optoelectronic devices based on epitaxial growth[10]. Their remarkable advantages aside, these lasers based on dielectric cavities are fundamentally limited as to how small they can be, owing to the diffraction limit of light. And this is where the real advantage of metal-based lasers begins: they can be fabricated with feature sizes comparable to those of modern transistors.

In 2003, David Bergman and Mark Stockman proposed the concept of a 'spaser' as an amplifier of localized surface plasmons oscillating at metal–dielectric interfaces[11]. Recently, this concept has been generalized to include travelling surface plasmon polariton amplifiers, or plasmonic nanolasers. In conventional semiconductor lasers, metal contacts are located far from the light emission regions and the cavity mode to prevent parasitic absorption; so, early on, the idea of using metals within the laser cavity seemed unconventional. Driven by the ongoing race to miniaturization, researchers are now able to fabricate nanolasers in unique architectures, including the metallic-coated nanolaser[12–20], plasmonic nanowire laser[21–37], metal–insulator–metal gap-mode nanolaser[38,39], metallic-nanoparticle laser[40–43], nanopatch laser[44], nanodisk laser[45], nanosquare laser[46–54], plasmonic crystal nanolaser[55–57], coaxial nanolaser[58,59], waveguide embedded plasmonic nanolaser[60], pseudowedge nanolaser[61], Tamm plasmon laser[62,63] and hyperbolic metacavity laser[64]. A characteristic in common of these nanolasers is the ability of metal nanostructures to confine light on a scale approaching or surpassing the diffraction limit. Key metrics of some representative nanolasers are shown in Table 1. Thanks to the limited number of optical modes in nanoscale cavities, the eigenmode of a nanolaser can be engineered in a controllable manner[65]. Furthermore, ensembles of nanolasers operating in unison can provide a macroscopic response, which provides a unique control over laser characteristics[66–74]. Figure 1 shows some representative micro- and nanolaser configurations. To capitalize on these proof-of-principle developments, we argue that the next phase of nanolaser research should focus primarily on practical applications.

In this Review, we look into the recent progress of nanolaser applications. We first describe the operation principles and intrinsic merits of these devices. We then consider applications in optical interconnects, near-field spectroscopy and sensing, optical probing for biological systems and far-field beam synthesis through near-field eigenmode engineering. We also highlight the scientific and engineering challenges that remain for forging nanolasers into powerful tools for nanoscience and nanotechnology.

Intrinsic merits of nanolasers

The intrinsic merits of nanolaser devices stem from their capability to localize electromagnetic fields at optical frequencies simultaneously in frequency, time and space (Fig. 1b).

Influence of laser volume on power consumption and threshold. One of the prime motivations for laser miniaturization is to reduce power consumption. In the early 1990s, it was realized that faster operation, lower threshold and power consumption could be achieved for the smallest lasers, for which there are very few cavity modes[75–77]. By reducing the number of excited states in lasers with small physical volumes, power consumption would be naturally minimized, but gains in efficiency were also predicted. For example, smaller lasers have fewer optical modes available to the gain medium, and this increases the spontaneous emission coupling factor, β, the fraction of spontaneous emission directed into

[1]State Key Lab for Mesoscopic Physics and School of Physics, Peking University, Beijing, China. [2]Collaborative Innovation Center of Quantum Matter, Beijing, China. [3]The Blackett Laboratory, Department of Physics, Imperial College London, London, UK. *e-mail: renminma@pku.edu.cn

Table 1 | Key metrics of various nanolasers

Year	Type	Feedback	Size	Gain medium	Emission wavelength	Pump	Temperature	Threshold	Refs
—	Typical VCSEL	Fabry–Pérot	Diameter: 10 μm Length: 1 μm	InGaAs/ GaAs	980 nm	Electrical, continuous wave	Room temperature	~1 kW cm^{-2}	93
2007	Metallic-coated pillar	Fabry–Pérot	Diameter: 210 nm Length: ~2 μm	InGaAs	1,400 nm	Electrical, continuous wave	77 K	~26 kW cm^{-2}	12
2009	Spaser	Localized SPR	Diameter: 44 nm	Dye	530 nm	Optical, pulsed	Room temperature	—	40
2009	Plasmonic nanowire	Fabry–Pérot	Diameter: ~100 nm Length: ~10 μm	CdS	490 nm	Optical, pulsed	10 K	~100 MW cm^{-2}	21
2009	Gap plasmon	Fabry–Pérot	Thickness: ~90 nm Length: 6 μm	InGaAs	1,500 nm	Electrical, continuous wave	10 K	~20 kW cm^{-2}	38
2010	Plasmonic nanodisk	Whispering gallery	Thickness: 235 nm Diameter: 0.9–1.2 μm	InAsP MQWs	1,300 nm	Optical, pulsed	8 K	~120 kW cm^{-2}	45
2010	Metallic-coated disk	Whispering gallery	Thickness: 480 nm Diameter: 490 nm	InGaAsP	1,430 nm	Optical, pulsed	Room temperature	~70 kW cm^{-2}	13
2010	MIM nanopatch	Dipole resonance	Thickness: 230 nm Diameter: 400–620 nm	InGaAsP	1,400 nm	Optical, pulsed	78 K	~80 kWcm^{-2}	44
2011	Plasmonic nanosquare	Whispering gallery	Thickness: 45 nm Length: 1 μm	CdS	500 nm	Optical, pulsed	Room temperature	~2 GW cm^{-2}	46
2012	Plasmonic coaxial	Fabry–Pérot	Diameter: 200 nm Height: 210 nm	InGaAsP MQWs	1,400 nm	Optical, continuous wave	4.5 K	–	58
2012	Plasmonic nanowire	Fabry–Pérot	Diameter: 60 nm Length: 480 nm	InGaN	510 nm	Optical, continuous wave	78 K	~3 kW cm^{-2}	22
2013	Metallic-coated pillar	Fabry–Pérot	Length: 1.39 μm Width: 1.15 μm Height: 1.7 μm	InGaAs	1,590 nm	Electrical, continuous wave	Room temperature	~100 kW cm^{-2}	18
2014	Plasmonic nanowire	Fabry–Pérot	Diameter: ~50 nm Length: ~200 nm	InGaN	468–642 nm	Optical, continuous wave	7 K	~100 W cm^{-2}	27
2014	Metallic-coated disk	Whispering gallery	Cavity volume: 3 μm^3	InGaAs	15 nm	Electrical, continuous wave	77 K	~30 kW cm^{-2}	19
2014	Plasmonic nanowire	Fabry–Pérot	Diameter: ~100 nm Length: ~15 μm	GaN	375 nm	Optical, pulsed	Room temperature	~3 MW cm^{-2}	26
2015	Plasmonic nanowire	Fabry–Pérot	Diameter: ~150 nm Length: ~5 μm	GaAs–AlGaAs	800 nm	Optical, pulsed	8 K	~1 kW cm^{-2}	28
2016	Plasmonic nanowire	Fabry–Pérot	Diameter: ~70 nm Length: ~1–4 μm	ZnO	380 nm	Optical, pulsed	Room temperature	~100 MW cm^{-2}	30
2017	Spaser	Localized SPR	Diameter: 22 nm	Dye	528 nm	Optical, pulsed	Room temperature	~3 MW cm^{-2}	43
2018	Plasmonic pseudo-wedge	Fabry–Pérot	Wedge length: 80 nm	ZnO	370 nm	Optical, pulsed	77 K	~55 MW cm^{-2}	61
2018	Hyperbolic metacavity	Whispering gallery	Length: 200 nm	AlGaN	290 nm	Optical, pulsed	Room temperature	~90 kW cm^{-2}	64

MQW, multi quantum well; MIM, metal–insulator–metal.

the laser mode. A larger β allows stimulated emission to start under weaker pump conditions, thus reducing laser threshold. In the extreme case in which there is only one mode available for laser action ($\beta \rightarrow 1$), thresholdless behaviour occurs with no clear phase transition between regimes in which spontaneous and stimulated emission dominate[58]. Alternative methods are then typically needed to identify the laser phase transition[20,59]. Box 1 discusses technical details of the threshold of small lasers.

Nanolaser dynamics. The strong spatial localization of nanocavity modes leads to modified dynamics due to enhanced interactions between the gain medium and the laser mode, known as the Purcell effect[78]. The Purcell effect changes the natural lifetime of spontaneous emission, τ_0, to $\tau = F^{-1}\tau_0$, where F is the Purcell factor. Moreover, emission into each available mode is modified by distinct amounts, where the emission lifetime into a particular mode is $F_m^{-1}\tau_0$. It is this preference for emission into certain modes that also leads to a modification of β. When the cavity resonance is broader than the emission linewidth and suitably tuned, the Purcell enhancement factor F_m is proportional to Q/V_m, where Q is the cavity quality factor and V_m is the effective optical volume of the laser mode[78]. In contrast, when the cavity resonance is narrower, then it is the emission linewidth and V_m that determine F_m rather than the cavity resonance linewidth[79]. The emission spectra of organic

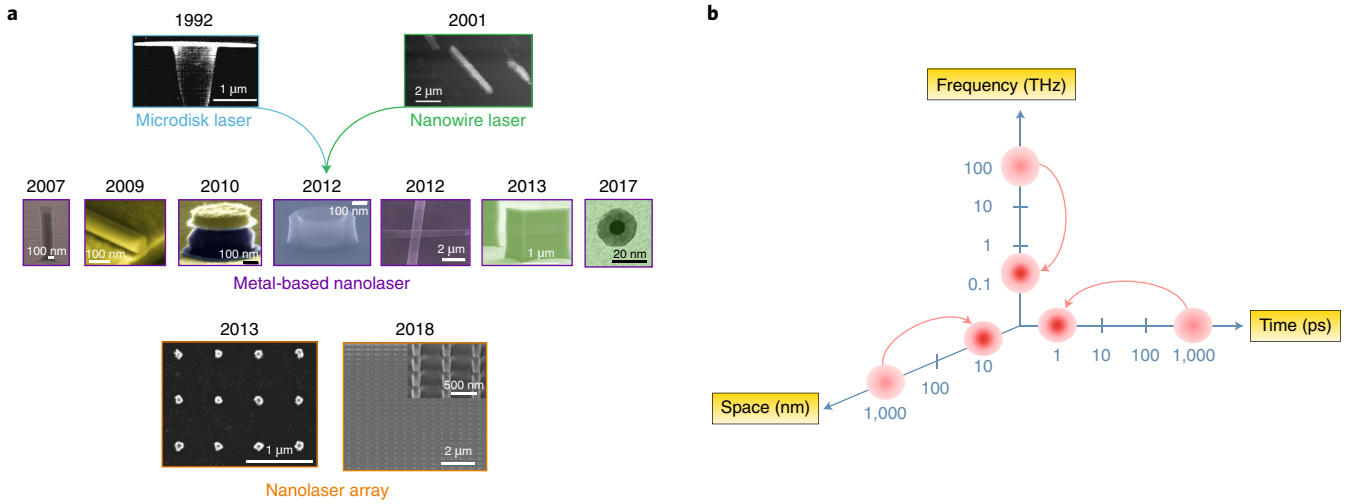

Fig. 1 | Development and intrinsic merits of nanolasers. a, First row: dielectric microdisk lasers and nanowire lasers; second row: representative metal-based nanolasers with various cavity configurations; third row: nanocavity array lasers. **b**, Nanolasers provide simultaneous localization of electromagnetic fields at optical frequencies in frequency, time and space. The lighter and darker red markers along the space axis indicate the wavelength of visible/near-infrared light in free space and the feature size of a nanolaser cavity, respectively. Along the frequency and time axes, the red markers compare the spectral bandwidth and lifetime of typical semiconductor gain materials in free space and for a nanolaser, respectively. Adapted from (**a**, first row, left) ref. [7], APS; (right) ref. [9], American Chemical Society; (middle row, left to right) ref. [12], SNL; ref. [21], SNL; ref. [44], OSA; ref. [58], SNL; ref. [60], American Chemical Society; ref. [18], OSA; ref. [43], SNL; (third row, left) ref. [66], SNL; (right) ref. [74], SNL.

dyes and inorganic semiconductors are a few tens of nanometres at room temperature, so the Purcell enhancement factors of nanocavities with quality factors less than about 100 can be estimated through Q/V_m.

The accelerated spontaneous emission into lasing modes enables nanolasers to have ultrafast responses[80], with a recent experimental demonstration of subpicosecond pulses[25]. While the Purcell effect accelerates light–matter interactions, it also increases the β factor, which further accelerates the temporal response under direct laser modulation[81–83]. Accessing high Purcell factors through high cavity quality is not valid when the cavity resonance is narrower than the inhomogeneously broadened emission linewidth. Furthermore, it is not necessarily advantageous in laser performance. For example, a long photon lifetime limits the modulation bandwidth of a laser[82].

Nanolaser spectral linewidth. The spectral width of metal-based nanolasers in a quasi-continuous pumping regime can be as narrow as about 0.3 nm (100 GHz) at 700 nm (ref. [48,84]), which is comparable to state-of-the-art semiconductor lasers with similar cavity lengths, such as vertical-cavity surface-emitting lasers (VCSELs). The relatively poor spectral density stems from their small gain volume and high spontaneous emission noise for the low number of optical modes in all small lasers. The advantage of nanolasers thus lies mainly in their capability to localize light in space, with a key figure of merit being the optical energy density. However, nanolasers can bring both sensitivity and spectral resolution to a variety of sensing applications, and so linewidth remains a key parameter of interest. Even the moderate spectral density of nanolasers is still far superior to incoherent light sources and thus vital for applications that exploit nanoscale localized optical fields as well as demanding coherence.

Nanolaser energy density. The optical mode volume, V_m, is another figure of merit often quoted in the field of plasmonics and nanophotonics, as it is related to the local optical density of states, which assesses the enhancement of the process of light–matter interaction[85]. However, the advantage of a nanolaser lies in its ability to generate optical energy within this volume directly. Because a laser makes use of light emission within its physical gain volume, V_{phy}, and delivers this to the laser mode volume, it is their ratio, V_{phy}/V_m, that is relevant.

For a semiconductor nanolaser under continuous-wave operation, the output power, P, can be related to the internal carrier density, n, and its dynamical parameters according to $P = \eta n h\nu \ V_{phy} / \tau_s$, assuming an external quantum efficiency η and a stimulated recombination lifetime τ_s. Above threshold, n is approximately the clamped threshold carrier density, while τ_s varies dependent on the pumping conditions. Predictions of the typical output power of a nanolaser under $\eta = 1$ as function V_{phy} and τ_s are shown in Fig. 2a. We note that the reduction in a nanolaser's physical volume accelerates the gain dynamics, τ_s, via the Purcell effect, which increases the emission power.

Under ultrafast pulsed optical pumping shorter than τ_s, gain switching can also lead to ultrashort output pulses. In this case, the peak power of a single pulse may be estimated when τ_s is taken as the output pulse width. For a single generated pulse, the intracavity energy density can be estimated to be $U = nh\nu V_{phy}/V_m$. The local energy density is thus proportional to V_{phy}/V_m. Whereas conventional nanolasers have values of V_{phy}/V_m close to unity, plasmonic nanolasers enable $V_{phy} \gg V_m$, allowing fairly high optical energy density to be achieved. Furthermore, plasmonic nanolasers tend to have higher threshold carrier densities compared with conventional semiconductor lasers, allowing energy densities $U > 50\ \mathrm{J\,cm^{-3}}$. In the case of gain switching on timescales of $\tau_s = 1$ ps, this can lead to peak pulsed intensities $I > 10^{11}\ \mathrm{W\,cm^{-2}}$ (ref. [25]).

The high local field intensities attainable within nanolasers can lead to various applications such as data storage, sensing, imaging, optical probing and spectroscopy at the optical near field. Furthermore, it is possible that nonlinear effects may emerge and play a role in both device operation and application; for example, intra-cavity frequency mixing. In these cases, the local optical energy spectral density ($\mathscr{U}$, in units of energy/volume) that a nanolaser generates inside its cavity is also a key figure of merit. Under pulsed gain switching operation, $\mathscr{U} = \frac{U}{\Delta\nu\,\Delta t}$, assuming a quantum efficiency of 100%, where $\Delta\nu$ is the spectral linewidth and

Box 1 | Threshold minimization of a laser

Early works in the 1990s identified the influence of laser size on lasing threshold[75–77]. An unambiguous definition of threshold is the condition in which the rates of spontaneous and stimulated emission into the laser mode are equal. A straightforward analysis of rate equations for a semiconductor laser in steady state leads to an expression for threshold photon density pump rate[53],

$$P_{\mathrm{th}} = \frac{h\nu}{\eta A}\frac{(1+\beta)}{2}\left[\frac{\gamma}{\beta\Gamma} + F\frac{2n_0 V_{\mathrm{phy}}}{\tau_0}\right] \quad (1)$$

where η_a is the proportion of pump power absorbed by the laser's gain medium; $h\nu$ is the photon energy of the emission; A is the area of the pump beam; γ is the cavity loss rate (excluding intrinsic loss due to the gain material); Γ is the overlap factor between the optical mode and the gain region; V_{phy} is the gain medium volume; $2n_0 = n_{\mathrm{inv}}$ is the carrier density at twice the transparency value; τ_0 is the natural spontaneous emission lifetime; F is the Purcell factor; and β is the spontaneous emission factor.

Two contributions to the threshold are evident in the square brackets of equation (1): the first term accounts for cavity mode loss, and the second accounts for the intrinsic loss of the gain material. We find that the ratio of cavity loss to material loss, $\zeta = \gamma\tau_0/(\beta F\Gamma n_{\mathrm{inv}} V_{\mathrm{phy}})$, is a useful parameter for characterizing the threshold of a laser. Accounting for the definition of ζ, we write equation (1) as

$$\Gamma R_{\mathrm{th}}/\gamma = (1+\beta^{-1})(1+\zeta^{-1})/2 \quad (2)$$

where $R_{\mathrm{th}} = \eta_a P_{\mathrm{th}} A/h\nu$ is the threshold rate of photon generation in the cavity, and $\Gamma R_{\mathrm{th}}/\gamma$ can be defined as a normalized threshold pump rate. Notably, the minimum pump rate, $R_{\mathrm{th}} = \gamma/\Gamma$, implies that photons must be supplied to the cavity as fast as they are being lost.

The definition of the normalized threshold pump rate allows us to isolate the roles of β and ζ in determining the threshold independently of a particular laser device. Clearly, laser threshold can be minimized in two ways: first, $\beta \to 1$, which demands a strong Purcell effect; and second, ζ must be maximized so that the total loss is cavity-loss dominated. Thus, β and ζ quantify the wastage of energy in attaining laser threshold: β measures energy lost as coupling to optical modes that do not lase, and ζ accounts for energy lost in achieving population inversion (see figure).

To adapt ζ to account for the various types of gain media in the literature, we define $\overline{N} = \Gamma n_{\mathrm{inv}} V_{\mathrm{phy}}$ as the number of excited emission centres required for the gain medium to become transparent to the cavity mode. Estimates for a variety of lasers are shown in the table, assuming that $\tau_0 \approx 10^{-9}$ s, which is typical for organic and inorganic semiconductor gain media.

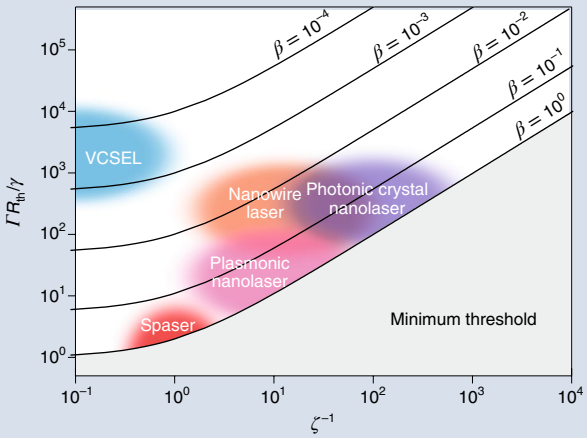

Normalized threshold as a function of the ζ and β parameters. The threshold energy consumption of a laser is determined by $\zeta^{-1} \propto V_{\mathrm{phy}}$. Reducing the volume of the laser always has a benefit provided that $\zeta < 1$

The table shows that semiconductor lasers typically have $\zeta < 1$, so that threshold is material-loss dominated. Maximizing ζ can lower the threshold, but a significant advantage is found only for $\zeta \to 1$. Increasing ζ beyond 1 is possible with quantum-well or quantum-dot gain materials or with a four-level gain mechanism; for example, quasi-four-level molecular gain. Because threshold decreases with $\zeta^{-1} \propto \overline{N}$, reducing the cavity volume, the carrier density at transparency or the overlap factors reduces a laser's energy consumption at threshold. This behaviour was observed recently in plasmonic lasers[53].

Notably, spasers operate under near-optimal conditions for energy consumption at threshold, since $\zeta \approx 1$ and $\beta \approx 1$, but with cavity-loss rates at 10^{14} s^{-1}, they extend the laser phenomenon to its absolute limits and generally require pulsed operation to avoid thermal damage to the device.

Parameters for typical small laser systems used to estimate the ratio of cavity and material losses, ζ

Type	γ (s^{-1})	βF	$\overline{N}$	ζ
Spaser	10^{14}	10^{2}	10^{3}	1
Plasmonic nanolaser	10^{13}–10^{14}	1–10	10^{5}	10^{-2}–1
Nanowire laser	10^{12}–10^{13}	10^{-2}–10^{-1}	10^{6}	10^{-2}–1
Photonic crystal laser	10^{11}–10^{12}	10–10^{2}	10^{3}	10^{-3}–10^{-1}
VCSEL	10^{11}–10^{12}	10^{-4}–10^{-3}	10^{5}	1–100

Δt is the pulse width. A nanolaser can directly generate strong local fields owing to its unique capability to localize optical radiation in time, space and frequency simultaneously. This would be maximal in the case of transform-limited pulses, which is a potential future research direction in nanolaser science.

Eigenmode engineering of nanolasers. Each laser mode is a specific eigenmode of a cavity. The number of eigenmodes (N) allowed in a cavity can be estimated by $N = \rho V_{\mathrm{phy}} \Delta\nu_E$, where ρ is the density states of the cavity, V_{phy} is the physical size of the cavity and $\Delta\nu_E$ is the gain spectrum bandwidth. Because $\Delta\nu_E$ is about a few tens of terahertz for typical organic dyes and semiconductor materials, generally only a few eigenmodes coincide spectrally with the gain spectrum when the laser cavity size is subwavelength-scale in all three dimensions. This enables one to engineer the eigenmode of a nanolaser in a controllable manner for synthesis of inner laser cavity fields and/or emission beams. Such eigenmode engineering is particularly important in nanolaser arrays, where laser eigenmodes are engineered at both the levels of single nanolaser cavity and structural periodicity, which provides a unique control over laser characteristics (see section on eigenmode engineering below)

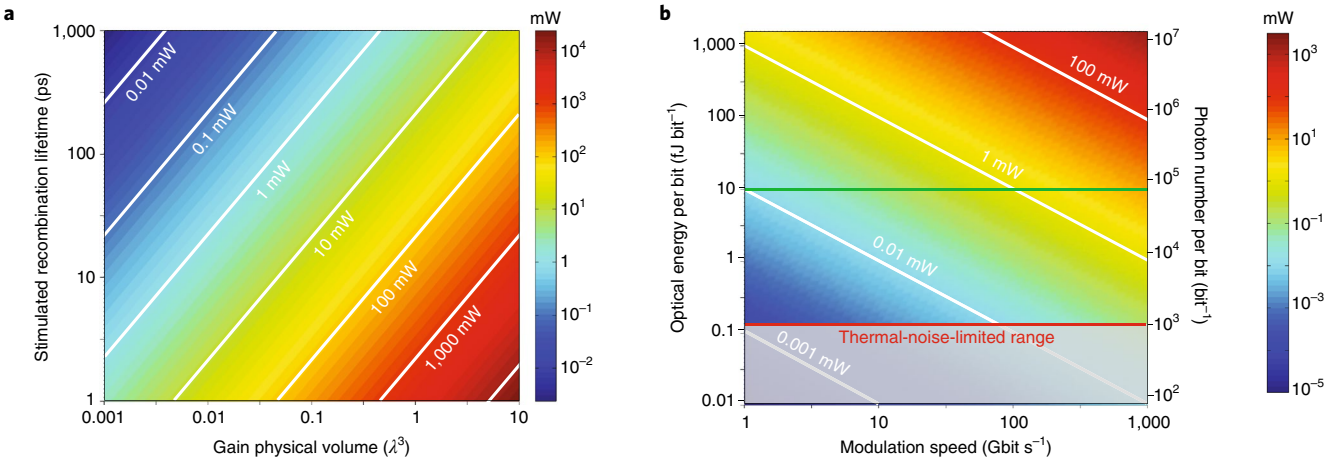

Fig. 2 | Relationships between light output power and key nanolaser parameters relevant to optical interconnects. a, The dependence of the emission power of a laser on its gain physical volume and stimulated recombination lifetime, τ_s, assuming 100% quantum efficiency at 1,550 nm, and a threshold carrier concentration of 5×10^{18} cm^{-3}. **b**, Relationship between the optical energy per bit, the modulation speed and the emission power of a laser operating at 1,550 nm. We note that the total energy per bit should consider the external quantum efficiency and also include the switching energy induced by the parasitic capacitance. The green line indicates the target energy budget (10 fJ bit^{-1}) of a laser driving on-chip optical interconnects. The red line indicates the output power needed to ensure sufficient signal-to-noise ratio beyond the thermal noise of an optical receiver (about 0.13 fJ bit^{-1}).

Nanolasers for integrated optical interconnects

Global Internet traffic, currently about 10^{21} bytes (1 Zb) per year, is increasing exponentially and so is the energy consumption for data communications[86,87]. Lowering energy consumption is therefore crucial to sustain a data-driven future society. Although long-haul optical links powered by edge-emitting lasers have far surpassed the capabilities of electrical links for many decades, VCSELs have emerged as the best solution for short-distance optical interconnects. Compared with edge-emitting lasers, VCSELs scale down the largest dimension from hundreds of micrometres to micrometres and lower the energy consumption from hundreds of picojoules per bit to hundreds of femtojoules per bit. Nowadays, VCSELs are gradually replacing electrical interconnects in data centres and supercomputers, with 300 million devices deployed since 1996[88]. Continued laser miniaturization is thus a natural approach to lowering energy consumption.

Practical applications of nanolasers in on-chip integrated optical interconnects would require: low power consumption but with receivable output power and high modulation rate; highly efficient laser-to-waveguide coupling; and continuous-wave electrically driven capability at room temperature. But achieving these requirements simultaneously is challenging, as we discuss next.

Energy per bit for a directly modulated nanolaser light source. The energy per bit is a key figure-of-merit for optical interconnects[87]. To replace mature on-chip electrical interconnects, the total system energy must be considerably lower than 1 pJ bit^{-1}. The target energy budget for an optical system's drive laser should approach 10 fJ bit^{-1} (ref. [89]). A laser consumes energy by operating above a threshold power consumption, in addition to the energy needed for modulation. Other factors such as modulation format and link budget should also be considered for a complete assessment of nanolaser power requirement for optical interconnects.

Considering a nanolaser threshold of 10 kW cm^{-2}, a diffraction-limited device area of $\lambda^2/4$ at $\lambda = 1.55$ μm gives a threshold power consumption of 5.6 μW, which is equivalent to 0.56 fJ per bit at a data rate of 10 Gb s^{-1}. Nanolasers with device areas smaller than $\lambda^2/4$ have been demonstrated in several configurations[12,13,17,22,38–40,43,44,53,58,61,64]. Further reductions in device volume will reduce the laser threshold energy overhead, but eventually there will be a trade-off between the laser cavity loss and the device volume. In fact, it has been argued that the threshold current densities of the smallest plasmonic nanoparticle lasers are much higher than commercialized laser diodes, owing to the higher metallic loss rate and the extremely small cross-sectional area of the cavity[90]. However, high loss is inevitable in any small laser: pure dielectric cavities are plagued by radiation loss, metallic cavities by ohmic loss. Consequently, there is an optimal balance for nanolasers between reduced power consumption and threshold intensity[53].

The output power of a communications laser can be estimated as the product of optical energy per bit and the modulation speed. Figure 2b shows the relationship between the optical energy per bit, the modulation speed and the emission power of a laser operating at 1.55 μm. At a given modulation speed, the emission power of a nanolaser has an upper bound for low power consumption (<10 fJ bit^{-1}) and a lower bound determined by the thermal noise at the optical receiver. The total energy per bit should consider the external quantum efficiency and also include the switching energy induced by the parasitic capacitance. The switching energy can be estimated as $E = \frac{1}{2}CV^2$, where C is the device capacitance and V is the operation voltage. A small capacitance is required for low power consumption. To achieve a small capacitance at femtofarad level, the footprint of the laser needs to be significantly smaller than 1 μm^2 for a 100-nm junction length and picosecond carrier recombination lifetime[91]. The capacitance also determines the upper bound of operation speed together with the resistance, R, of the device, with the maximum modulation speed being less than $(2RC)^{-1}$.

The lower bound of the output power of a laser is determined by the sensitivity of an optical receiver. Typically, about 1,000 photons per bit are required for sufficient signal-to-noise ratio above thermal detector noise, assuming a 100% internal quantum efficiency[92]. For a link operating at a wavelength of 1.55 μm (0.8 eV), this corresponds to 0.13 fJ per bit (red line in Fig. 2b). At a bit rate of 10 Gb s^{-1}, this would require an average emissive power of 1.28 μW, which places a restriction on how small a nanolaser can be for optical interconnects, as shown in Fig. 2b.

A related metric is the external quantum efficiency (EQE), which measures the total energy per bit associated with heat generation and dissipation. Recent experiment shows that the EQE of a plasmonic nanolaser can exceed 10% at room temperature[84]. We believe

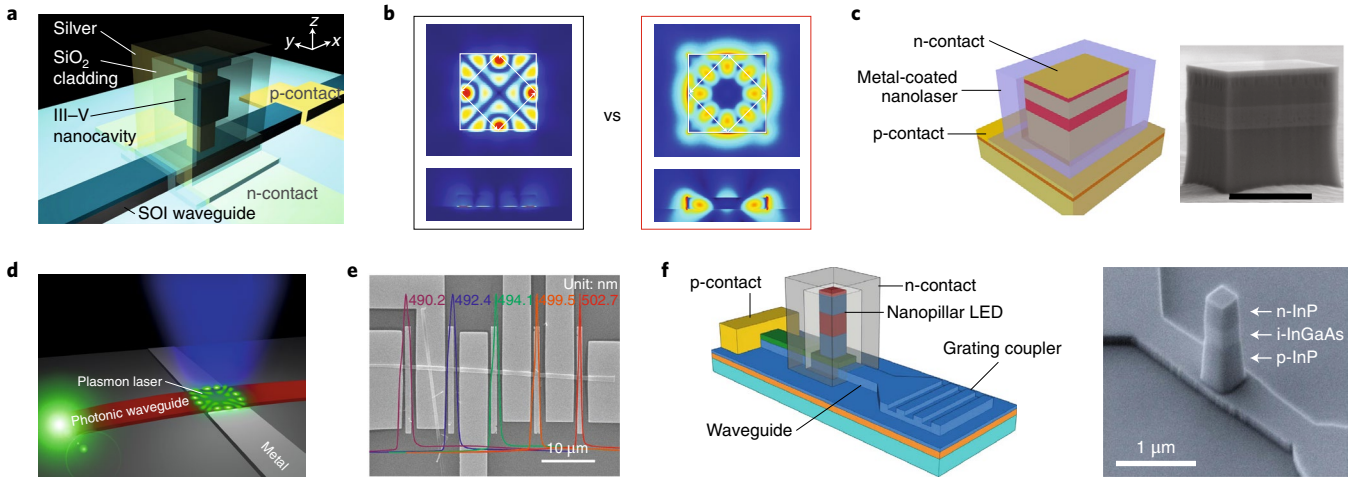

Fig. 3 | Nanolasers for optical interconnects. a, A proposed electrically driven metal-based nanolaser coupled to a waveguide for optical interconnects[94] SOI, silicon on insulator. **b**, Recent experimental work shows that power consumption in metal-based lasers can be lower than purely dielectric devices at nanoscale because of the tighter field confinement[53]. Electric field profiles of a plasmonic cavity mode (left) and a photonic cavity mode (right) with same gain size of 700 × 700 × 100 nm. **c**, Schematic and scanning electron microscope (SEM) images of a metal-coated nanolasers operating at room temperature under continuous electrically driving conditions[18]. Scale bar in SEM image, 1 μm. **d**, **e**, Schematic of a waveguide-embedded (WEB) plasmonic nanolaser with high-efficiency coupling of the cavity mode to the waveguide (**d**), and a photonic circuit based on a WEB plasmonic nanolaser array providing multiplexed emission wavelengths (**e**)[60]. **f**, Schematic and SEM images of metal-cavity light-emitting diodes based on InP on silicon substrate[95]. Reproduced from ref. [53], SNL (**b**); ref. [18], OSA (**c**); ref. [60], American Chemical Society (**d**,**e**); ref. [95], SNL (**f**, left); adapted from ref. [94], OSA (**a**); ref. [95], SNL (**f**, right).

that, although rarely studied in the nanolaser literature, this parameter deserves more attention when evaluating nanolasers for real-life applications, including near-field spectroscopy and sensing, integrated optical interconnects, solid-state lighting and free-space optical communication.

It is predicted that, owing to their subwavelength-size and low-quality cavities, plasmonic nanolasers can provide modulation bandwidths over hundreds of gigahertz[82]. Although the ultra-narrow pulse width observed in gain-switched nanolasers[25] suggests that ultra-high modulation bandwidth is possible, more research is needed to study electrical modulation of nanolasers. In particular, turn-on delay time jitter, relaxation resonance and excited carrier relaxation are all important characteristics that have yet to be explored[93].

Guiding of nanolaser radiation. The large momentum mismatch between light inside a deep subwavelength nanocavity and in free space results in the laser mode being diffracted in all directions. Nanoscale lasers that are allowed to radiate to free space consequently exhibit low collection efficiency. This can be rectified by coupling nanoscale laser emission to waveguide modes, as shown in Fig. 3a,d (refs [60,94]). For example, recently demonstrated waveguide-embedded plasmonic nanolasers enable over 70% coupling efficiency into waveguide modes (Fig. 3d,e)[60]. The metal-based lasers adopted in the waveguide-embedded plasmonic nanolasers have lower power consumption than conventional lasers at the nanoscale (Fig. 3b)[53].

Electrical injection. Optical interconnects require small electrically driven lasers, which inevitably require metal contacts. The idea of combining an electrical contact with light feedback and confinement is a compelling way to achieve a compact nanolaser, especially considering the difficulties in contacting purely dielectric devices such as photonic crystal and nanowire lasers. Besides the electrical interface and field confinement, the metal also serves as a heat sink, which is crucial for stable laser operation. A number of metal-clad electrically driven nanolasers have been demonstrated[12,16–19,38], and recently, room-temperature continuously driven devices were realized with a cavity volume of only $0.67\lambda^3$ ($\lambda = 1.59$ μm) (Fig. 3c)[18]. These metal-clad nanolasers are the smallest electrically driven lasers yet. Moreover, waveguide-coupled nanoscale light-emitting diodes (nanoLEDs) were realized on silicon substrate. Although the nanoLED does not lase, the device platform is promising as an integrated light source for optical interconnects (Fig. 3f)[95]. Despite recent progress, electrically injected nanolasers with performance relevant to practical applications (high thermal stability, integration and high coupling efficiency with waveguides and direct modulation with bandwidths over tens of gigahertz) are still challenging to achieve.

Nanolasers for sensing

Surface plasmon resonance sensors are now a prominent tool in biochemical sensing and detection[96]. However, a fundamental limitation of surface plasmon sensors is their strong radiative and non-radiative damping, which weakens the plasmon resonance and limits sensitivity. A consequence of damping is that plasmon resonances across the visible and near-infrared exhibit wide linewidths of tens to hundreds of nanometres, which limits sensing performances. These dampings can be fully compensated by gain medium in a plasmonic nanolaser cavity, which can narrow the plasmonic resonance linewidth by two orders of magnitude (Fig. 4a)[48].

Gas-phase nanolaser sensors. Plasmonic nanolaser sensors have recently been demonstrated that can detect specific molecules in air under normal conditions with sub-part-per-billion sensitivity (Fig. 4b)[47]. In a particularly instructive example, two explosive molecules, 2,4-dinitrotoluene and ammonium nitrate, were detected. The sensing mechanism relies on gas molecules modifying the surface recombination velocity of a plasmonic nanolaser gain material. Here, a semiconductor slab with an atomically smooth surface serves as the gain material, feedback geometry and sensing medium simultaneously. The large surface area to physical volume ratio of the nano-cavity, which is inversely proportional to the nano-slab thickness, ensures that any modulation of the surface chemistry will

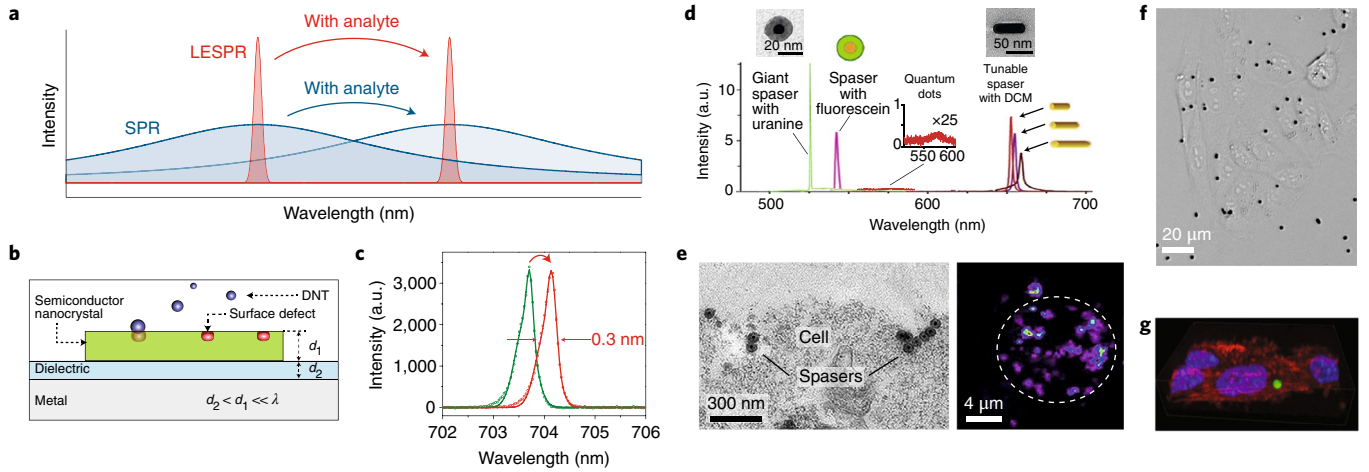

Fig. 4 | Near-field applications of nanolasers. a, Lasing-enhanced surface plasmon resonance (LESPR) has much narrower linewidth than its passive counterpart of surface plasmon resonance (SPR), enabling superior performance in sensing and detection[48]. **b**, Schematic of a plasmonic nanolaser sensor for detection of explosives, with sub-part-per-billion sensitivity[47]. DNT, 2,4-dinitrotoluene. **c**, LESPR for refractive index sensing[48]. The spectrum of a nanolaser shifts with the refractive index in the fully lasing state. a.u., arbitrary units. **d**, **e**, Plasmonic nanolasers with diameters down to 20 nm used as biological probes[43]. Transmission electron microscopy (TEM) of spherical and rod-like spasers, and their corresponding lasing emission spectra (**d**). DCM, 4-(dicyanomethylene)-2-methyl-6-(4dimethylaminostyryl)-4Hpyran. TEM image of single and clustered spasers on a breast cancer cell membrane after 30 min cell incubation at 37 °C (left); photothermal image of cancer cell labelled with spasers (right, false colours) (**e**). **f**, **g**, Microdisk lasers for cellular labelling and tracking[105]. Optical image of laser particles inside a living cell (**f**). Three-dimensional fluorescent image of a laser particle inside a cell, where green, blue and red colours indicate laser particle, nuclei and actin filaments, respectively (**g**). Reproduced from ref. [48], De Gruyter (**a**, **c**); ref. [105], OSA (**f**); adapted from ref. [47], SNL (**b**); ref. [43], SNL (**d**, **e**); ref. [105], OSA (**g**).

strongly affect the laser emission intensity. Although the large surface area favours analyte adsorption, the small physical volume of active material limits the number of carriers to be modulated inside.

Nanolaser sensors in biochemical-compatible environments. Surface plasmon refractive index sensors are the most extensively used optical biosensors. Recently, plasmonic nanolasers have also been demonstrated as refractive index sensors offering greatly improved sensitivity (Fig. 4c)[48,52], thanks to the high spectral coherence of lasing surface plasmons (<0.3 nm at $\lambda = 700$nm). For intensity-based sensing, the figure of merit for plasmonic nanolaser sensors can be around 84,000, which is about 400 times higher than state-of-the-art surface plasmon resonance sensors[96]. The high figure of merit was possible because of the high spectral coherence and high signal-to-noise ratio due to a greatly suppressed background emission and the steep tails of the Gaussian-shaped laser spectrum. The performance of plasmonic nanolaser sensors, especially for the wavelength sensing, can be further improved when a plasmonic nanocavity with even smaller mode volume and larger overlap between optical field and analytes is used[48,57,97]. In a plasmonic nanotrench laser, the mode volume can already be as small as about $5 \times 10^{-4}\lambda^3$, with a figure of merit greater than 1,000 for wavelength sensing at the lasing wavelength of $\lambda = 373$ nm (ref. [57]).

In a biochemical-compatible environment, plasmonic nanolaser sensors may experience fast degradation due to the reaction of photogenerated carriers with active sites at the crystal surface[52]. A step of surface passivation is necessary for improving their stability, and a recent experiment demonstrates that plasmonic nanolaser sensors with a 7-nm Al_2O_3 passivation layer show no observable degradation in hours, whereas without the passivation layer the nanolaser can only last for a few seconds[52].

Nanolasers for biological applications

Nanolasers have small physical volumes and can deliver optical energy to even smaller mode these volumes with simultaneously spectral and temporal optical localization. This enables a range of biological applications, including biological probing, cellular labelling and tracking, and super-resolution imaging.

Spasers as biological probes. Detection of laser-excited spontaneous emission from fluorescent labels remains a widely used biological imaging tool to study individual biomolecules and cells. However, optical saturation at high laser intensity, photobleaching and blinking effects limit the detection sensitivity and practicality. Stimulated emission in small lasers can be used to suppress photobleaching and blinking effects for a bright light emission with much narrower linewidth. Recently, the versatile functionalities of spasers were shown in complex biological backgrounds, from cellular cytoplasm in vitro to mouse tissue in vivo[43] (Fig. 4d,e). The diameter of the spaser is only 22 nm, with a gold core of about 10 nm diameter and a silica shell, about 6 nm thick, embedded with organic dye molecules. Under single nanosecond pulsed laser pumping, the spasers can provide super-bright stimulated emission, high photoacoustic imaging contrast and potential for photothermal destruction of cancer cells.

Microdisk lasers for cellular labelling and tracking. Microlasers have been demonstrated in biosystems with much narrower linewidth than fluorescent probes. These microlasers can serve as optical probes in biomedical imaging, cytometry, high-contrast cancer screening, immune-diagnosis, and cellular labelling and tracking[98–104]. Recently, free-standing microdisk laser particles from III–V compound semiconductors of InAlGaAs and InGaAsP were reported[105]. These microdisk lasers, with radius of about 1 μm, are coated with biocompatible materials. On optical pumping at 1,060 nm, they generate single-mode lasing with linewidths less than 1 nm and emission wavelength spanning from 1,200 nm to 1,600 nm with varied compositions of gain material. These laser particles can be internalized by cells, and their emission remains stable over the course of repeated measurements (Fig. 4f,g)[105]. Highly multiplexed optical barcodes with roughly 400 spectral channels have been demonstrated, showing the great potential

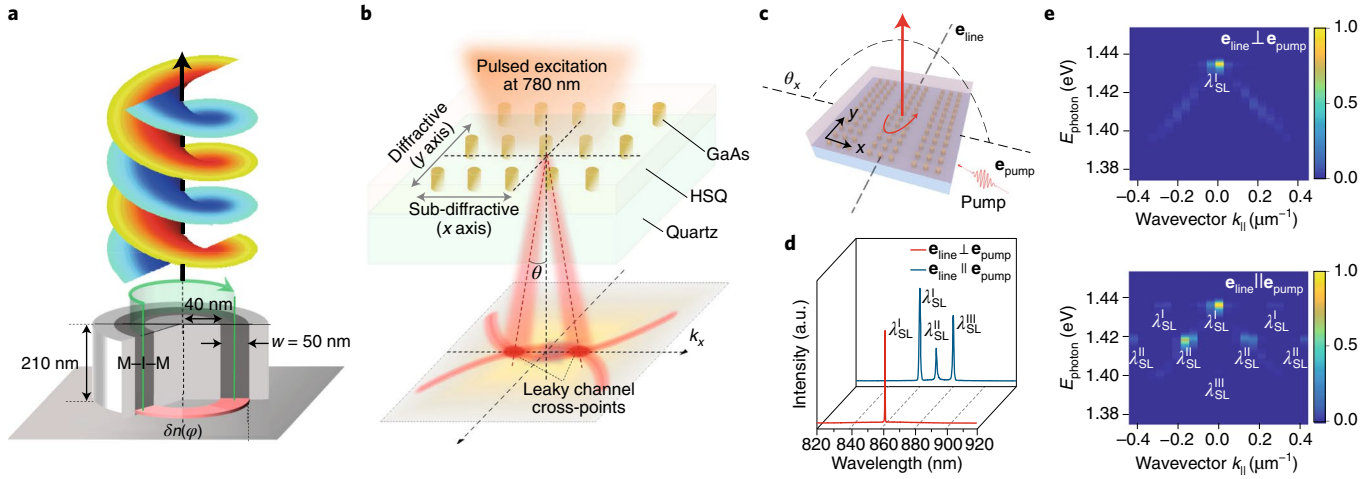

Fig. 5 | Eigenmode engineering of nanolasers. a, Direct optical vortex emission from a chiral plasmonic nanocavity[65]. **b**, Directional lasing in resonant semiconductor nanoantenna arrays[74]. **c**, Plasmonic nanocavity array laser in a superlattice configuration[71]. **d**, Lasing emission from gold nanoparticle arrays tuned in real time by changing the pump laser orientation[71]. **e**, Multi-mode lasing in plasmonic superlattices enabling control over spectrum and direction in the far field[71]. HSQ, hydrogensilsesquioxane. e_{line} and e_{pump}, the directions of the line axis and pump polarization. SL, superlattice. Reproduced from ref. [65], https://arxiv.org/abs/1707.01055 (**a**); adapted from ref. [74], SNL (**b**); ref. [71], SNL (**c**–**e**).

of small lasers in the application of multiplexed cellular labelling and tracking.

Super-resolution imaging. An optical microscopy technique that uses the intrinsically nonlinear laser process of nanolasers for super-resolution imaging has recently been introduced[106]. Around lasing threshold, lasers exhibit nonlinear light output versus input power owing to the phase transition from spontaneous-emission-dominated operation to stimulated emission. This nonlinear power dependence from a nanolaser can be made to yield a spatial resolution around 5 times higher under the lasing condition than for the same device operated below lasing threshold. In another approach, a fluorescent nanowire ring was demonstrated to produce omnidirectional evanescent wave illumination, enabling wide-field far-field subdiffraction imaging[107]. Such a technique is label-free and can be conveniently integrated with conventional microscopes, which expands the flexibility of nanoscale light sources for imaging applications.

Nanolasers for far-field applications

So far, we have discussed how individual nanolasers produce light that accesses the nanoscale in some manner. However, as mentioned above, the eigenmode of a nanolaser can be engineered in a controllable manner for synthesis of the inner laser cavity field and/or emission beam. Furthermore, ensembles of nanolasers operating in unison can provide a macroscopic response that would not be possible in conventional lasers. In this case, it is the structure at the nanoscale that determines a laser's operational characteristics, in a manner similar to a metamaterial. In the near field, the polarization and profile of each nanolaser eigenmode can be controlled, with additional control over the ensemble through coupling, relative phase, eigenmode symmetry and topology. Such cooperative eigenmode engineering is distinct from photonic crystal lasers where periodicity is the main control parameter, and could enable unprecedented control of the macroscopic laser field with a range of far-field applications.

Eigenmode engineering in a single nanocavity. Owing to their specific spatial structure and associated orbital angular momentum, optical vortices or phase singularities are receiving increasing attention from the optics community[108] and have been exploited for many important applications, including optical trapping, optical manipulation, metrology, imaging and free-space communication[109]. Recently, general methods to control the optical eigenmodes of a microcavity with vortex radiation have emerged[110,111]. Vortex laser eigenmodes synthesized in a micro-ring cavity at an exceptional point can produce a stable vortex beam[110]. Such a system can generate different vortex orders by modulating the grating on the micro-ring cavity[111].

A recent study has shown that a chiral plasmonic nanocavity at an exceptional point can be used for constructing thresholdless vortex nanolasers (Fig. 5a)[65]. Such a chiral plasmonic nanocavity can twist the emission of a single emitter to produce vortex radiation with β factor close to unity and Purcell factor over 1,000. More interestingly, when interacting with a single dipole emitter, a counterintuitive phenomenon emerges in which the radiation field of the dipole can display the opposite handedness to the coalesced eigenstate of the system at the exceptional point[65].

Band engineering of semiconductor resonator lattice. Compared with their thin-film counterparts, semiconductor nanowires have superior strain relaxation ability, which presents excellent opportunities for silicon photonics. Recently, selective-area epitaxy technology has been used to grow well-defined InGaAs nanowire array lasers on a silicon-on-insulator platform, forming one-dimensional photonic crystal nanobeam cavities[73]. Single-mode lasing has been demonstrated in the nanowire arrays through optical pumping. The emission wavelength of the nanowire array laser is tunable by the simple adjustment of the lithographically defined growth pattern.

Bound states in the continuum (BICs) are eigenmodes that remain localized despite lying inside the continuous spectrum of radiation waves. It has been proven that BIC states can be polarization singularities in momentum space and that they are inherently topologically protected[112]. Recently, laser action of BIC supported by a cylindrical semiconductor resonator lattice has been demonstrated[113]. Using the feedback mechanism of BIC, dielectric nanoantenna arrays with deep-subwavelength resonator units can perform directional lasing with a low threshold and high quality factor (Fig. 5b)[74]. In nanoantenna array lasers, the unit resonator has a diameter of only 100 nm and a height of 250 nm, while the emission wavelength is about 830 nm. BIC lasers can be robust and scalable with persistent single-mode lasing for various radii and array

sizes. Such lasers could also eventually enable phased array operation for laser beam steering, high-power semiconductor lasers and other applications.

Most recently, topological insulator lasers have been experimentally demonstrated. The topologically protected edge states create a robust lasing mode[114–117]. Notably, the dipole and quadrupole modes accommodated on a hexagonal cluster, composed from six dielectric pillars, can be degenerate in frequency in a two-dimensional hexagonal lattice, generating Dirac-like photonic dispersion of a honeycomb photonic crystal[118]. By enhancing the coupling strength between these clusters, this degeneracy can be lifted, and a band inversion between dipole and quadrupole modes takes place, resulting in a topological photonic state. These results not only reveal that photonic crystals with nontrivial topology can be constructed based on purely dielectric materials, but also demonstrate eigenmode engineering with cooperative consideration at both levels of unit cell and structure periodicity.

Band engineering of metal particle arrays. The concept of using an array of coupled lasing sub-units for directional emission was originally proposed for split-ring resonators at mid-infrared wavelengths[119]. Experimental realization was recently achieved in the near-infrared but with simpler systems of metal nanoparticle arrays embedded in an organic gain medium and metal hole arrays on semiconductor slabs[66–72]. In the nanoparticle array, each small metal nanoparticle can be treated as a dipole emitter radiating spherical waves. However, interference of dipolar radiation in the far field introduces sharp lattice resonances that are distinct from band edge modes of periodic dielectric structures, for example, in distributed feedback lasers. Periodic metal nanoparticle arrays in a homogeneous dielectric environment exhibit an isolated lattice plasmon state characterized by suppressed radiative loss and subwavelength localized fields around the nanoparticles.

Periodic arrays of metal nanoparticles coupled with organic gain molecules can now be operated at room temperature with excellent spectral and spatial coherence[66]. A remarkable advantage of lasing in nanoparticle arrays is their wide-range tunability: in a nanoparticle array laser, the solution-based organic gain molecules are dynamically changeable, and the lattice plasmon resonance is robust yet mechanically stretchable[68,72]. Recently, access to controlled multimodal lasing at different frequencies was also realized by plasmonic superlattices, finite-sized nanoparticle patches arranged on a larger periodicity (Fig. 5c–e)[71]. The multimodal lasing behaviour of superlattice plasmon modes can be uniquely controlled by manipulating near-field intensities and individual mode quality, and the emission angle of beams can be controlled by engineering the superlattice.

Outlook

From the point of view of fundamental physics, almost all the elements are in place to exploit nanolasers in a broad variety of applications. The challenges remaining are engineering ones needed to attain the level of performance required. In particular, on-chip optical interconnects will require electrically injected nanolasers with low power consumption and other specific key targets, such as direct modulation speed, thermal stability and wall-plug efficiency, and coupling efficiency to an integrated waveguide. However, there are numerous nanolaser applications that do not require electrical injection, especially near-field applications, in which nanolasers can be exploited for their unique capability to achieve high optical energy densities by simultaneous spatial, temporal and spectral confinement. This could enable various spectroscopies, usually restricted to optical laboratories, to be used in portable devices. Cavity configuration engineering and metal quality improvements are crucial to improve the performance of nanolasers, but a more pressing challenge concerns the compatibility and implementation of nanolasers within existing systems and protocols. Consequently, collaboration between academic communities and industry is of great importance. Nanolaser arrays for far-field applications also represent an intriguing emerging area that can lead to high-power semiconductor lasers with high modulation speed. It could also allow optical beam manipulation such as steering and shaping, providing a controllable radiation phase of individual nano-antennas.

Received: 13 November 2017; Accepted: 31 October 2018;
Published online: 17 December 2018

References

1. Maiman, T. H. Stimulated optical radiation in ruby. *Nature* **187**, 493–494 (1960).
2. *What is NIF?* https://lasers.llnl.gov/about/what-is-nif
3. Genet, C. & Ebbesen, T. W. Light in tiny holes. *Nature* **445**, 39–46 (2007).
4. Schuller, J. A. et al. Plasmonics for extreme light concentration and manipulation. *Nat. Mater.* **9**, 193–204 (2010).
5. Stockman, M. I. Nanoplasmonic sensing and detection. *Science* **348**, 287–288 (2015).
6. Stockman, M. I. et al. Roadmap on plasmonics. *J. Opt.* **20**, 043001 (2018).
7. McCall, S. L., Levi, A. F. J., Slusher, R. E., Pearton, S. J. & Logan, R. A. Whispering-gallery mode microdisk lasers. *Appl. Phys. Lett.* **60**, 289–291 (1992).
8. Painter, O. et al. Two-dimensional photonic band-gap defect mode laser. *Science* **284**, 1819–1821 (1999).
9. Johnson, J. C. et al. Single nanowire lasers. *J. Phys. Chem. B* **105**, 11387–11390 (2001).
10. Eaton, S. W., Fu, A., Wong, A. B., Ning, C.-Z. & Yang, P. Semiconductor nanowire lasers. *Nat. Rev. Mater.* **1**, 1–11 (2016).
11. Bergman, D. J. & Stockman, M. I. Surface plasmon amplification by stimulated emission of radiation: Quantum generation of coherent surface plasmons in nanosystems. *Phys. Rev. Lett.* **90**, 027402 (2003).
12. Hill, M. T. et al. Lasing in metallic-coated nanocavities. *Nat. Photon.* **1**, 589–594 (2007). **This work demonstrates a metal-based nanolaser.**
13. Nezha, M. P. et al. Room-temperature subwavelength metallo-dielectric lasers. *Nat. Photon* **4**, 395–399 (2010).
14. Lu, C.-Y., Chang, S. W., Chuang, S. L., Germann, T. D. & Bimberg, D. Metal-cavity surface-emitting microlaser at room temperature. *Appl. Phys. Lett.* **96**, 251101 (2010).
15. Kim, M. W. & Ku, P.-C. Lasing in a metal-clad microring resonator. *Appl. Phys. Lett.* **98**, 131107 (2011).
16. Ding, K. et al. Room-temperature continuous wave lasing in deep-subwavelength metallic cavities under electrical injection. *Phys. Rev. B* **85**, 041301(R) (2012).
17. Ding, K. et al. An electrical injection metallic cavity nanolaser with azimuthal polarization. *Appl. Phys. Lett.* **102**, 041110 (2013).
18. Ding, K. et al. Record performance of electrical injection sub-wavelength metallic-cavity semiconductor lasers at room temperature. *Opt. Express* **21**, 4728–4733 (2013).
19. Gu, Q. et al. Amorphous Al_2O_3 shield for thermal management in electrically pumped metallo-dielectric nanolasers. *IEEE J. Quant. Electron.* **50**, 499–509 (2014).
20. Pan, S. H., Gu, Q., Amili, A. E., Vallini, F. & Fainman, Y. Dynamic hysteresis in a coherent high-β nanolaser. *Optica* **3**, 1260–1265 (2016).
21. Oulton, R. F. et al. Plasmon lasers at deep subwavelength scale. *Nature* **461**, 629–632 (2009). **This work demonstrates a plasmonic nanowire laser.**
22. Lu, Y. J. et al. Plasmonic nanolaser using epitaxially grown silver film. *Science* **337**, 450–453 (2012).
23. Liu, X., Zhang, Q., Yip, J. N., Xiong, Q. & Sum, T. C. Wavelength tunable single nanowire lasers based on surface plasmon polariton enhanced Burstein–Moss effect. *Nano Lett.* **13**, 5336–5343 (2013).
24. Wu, X. et al. Hybrid photon–plasmon nanowire lasers. *Nano Lett.* **13**, 5654–5659 (2013).
25. Sidiropoulos, T. et al. Ultrafast plasmonic nanowire lasers near the surface plasmon frequency. *Nat. Phys.* **10**, 870–876 (2014).
26. Zhang, Q. et al. A room temperature low-threshold ultraviolet plasmonic nanolaser. *Nat. Commun.* **5**, 4953 (2014).
27. Lu, Y. J. et al. All-color plasmonic nanolasers with ultralow thresholds: autotuning mechanism for single-mode lasing. *Nano Lett.* **14**, 4381–4388 (2014).
28. Ho, J. F. et al. Low-threshold near-infrared GaAs–AlGaAs core–shell nanowire plasmon laser. *ACS Photonics* **2**, 165–171 (2015).
29. Ho, J. et al. A nanowire-based plasmonic quantum dot laser. *Nano Lett.* **16**, 2845–2850 (2016).
30. Chou, Y. H. et al. High-operation-temperature plasmonic nanolasers on single-crystalline aluminium. *Nano Lett.* **16**, 3179–3186 (2016).

31. Yu, H. C. et al. Organic–inorganic perovskite plasmonic nanowire lasers with a low threshold and a good thermal stability. *Nanoscale* **8**, 19536–19540 (2016).
32. Zhang, Q. et al. Wavelength tunable plasmonic lasers based on intrinsic self-absorption of gain material. *ACS Photonics* **4**, 2789–2796 (2017).
33. Yu, H. et al. Influence of silver film quality on the threshold of plasmonic nanowire lasers. *Adv. Optical Mater.* **5**, 1600856 (2017).
34. Lee, C. T. et al. Low-threshold plasmonic lasers on a single-crystalline epitaxial silver platform at telecom wavelength. *ACS Photonics* **4**, 1431–1439 (2017).
35. Kress, S. J. P. et al. A customizable class of colloidal-quantum-dot spasers and plasmonic amplifiers. *Sci. Adv.* **3**, e1700688 (2017).
36. Lu, J. et al. Plasmon-induced accelerated exciton recombination dynamics in ZnO/Ag hybrid nanolasers. *ACS Photonics* **4**, 2419–2424 (2017).
37. Liu, S. et al. Molecular beam epitaxy of single-crystalline aluminum film for low threshold ultraviolet plasmonic nanolasers. *Appl. Phys. Lett.* **112**, 231904 (2018).
38. Hill, M. T. et al. Lasing in metal–insulator–metal sub-wavelength plasmonic waveguides. *Opt. Express* **17**, 11107–11112 (2009).
39. Nguyen, N. B. et al. Hybrid gap plasmon GaAs nanolasers. *Appl. Phys. Lett.* **111**, 261107 (2017).
40. Noginov, M. A. et al. Demonstration of a spaser-based nanolaser. *Nature* **460**, 1110–1112 (2009).
41. Meng, X. G., Kildishev, A. V., Fujita, K., Tanaka, K. & Shalaev, V. M. Wavelength-tunable spasing in the visible. *Nano Lett.* **13**, 4106–4112 (2013).
42. Zhang, C. et al. Plasmonic lasing of nanocavity embedding in metallic nanoantenna array. *Nano Lett.* **15**, 1382–1387 (2015).
43. Galanzha, E. I. Spaser as a biological probe. *Nat. Commun.* **8**, 15528 (2017).
This work introduces a spaser for biological probing.
44. Yu, K., Lakhani, A. & Wu, M. C. Subwavelength metal-optic semiconductor nanopatch lasers. *Opt. Express* **18**, 8790–8799 (2010).
45. Kwon, S. H. et al. Subwavelength plasmonic lasing from a semiconductor nanodisk with silver nanopan cavity. *Nano Lett.* **10**, 3679–3683 (2010).
46. Ma, R. M., Oulton, R. F., Sorger, V. J., Bartal, G. & Zhang, X. Room-temperature sub-diffraction-limited plasmon laser by total internal reflection. *Nat. Mater.* **10**, 110–113 (2011).
47. Ma, R.-M., Ota, S., Li, Y., Yang, S. & Zhang, X. Explosives detection in a lasing plasmon nanocavity. *Nat. Nanotech.* **9**, 600–604 (2014).
48. Wang, X.-Y. et al. Lasing enhanced surface plasmon resonance sensing. *Nanophotonics* **5**, 52–58 (2016).
This work introduces plasmonic nanolaser for sensing in a biochemical environment.
49. Guo, C.-C., Xiao, J.-L., Yang, Y.-D., Zhu, Z.-H. & Huang, Y.-Z. Lasing characteristics of wavelength-scale aluminum/silica coated square cavity. *IEEE Photonics Technol. Lett.* **28**, 217–220 (2016).
50. Liu, N. Lithographically defined, room temperature low threshold subwavelength red-emitting hybrid plasmonic lasers. *Nano Lett.* **16**, 7822–7828 (2016).
51. Chen, H.-Z. et al. Imaging the dark emission of spasers. *Sci. Adv.* **3**, e1601962 (2017).
52. Wang, S. et al. High-yield plasmonic nanolasers with superior stability for sensing in aqueous solution. *ACS Photonics* **4**, 1355–1360 (2017).
53. Wang, S. et al. Unusual scaling laws for plasmonic lasers beyond diffraction limit. *Nat. Commun.* **8**, 1889 (2017).
This work clarifies the viability of metal confinement and feedback strategies in laser technology.
54. Huang, C. et al. Formation of lead halide perovskite based plasmonic nanolasers and nanolaser arrays by tailoring the substrate. *ACS Nano* **12**, 3865–3874 (2018).
55. Lakhani, A. M., Kim, M. K., Lau, E. K. & Wu, M. C. Plasmonic crystal defect nanolaser. *Opt. Express* **19**, 18237–18245 (2011).
56. Keshmarzi, E. K., Tait, R. N. & Berini, P. Single-mode surface plasmon distributed feedback lasers. *Nanoscale* **10**, 5914–5922 (2018).
57. Cheng, P.-J. et al. High-performance plasmonic nanolasers with a nanotrench defect cavity for sensing applications. *ACS Photonics* **5**, 2638–2644 (2018).
58. Khajavikhan, M. et al. Thresholdless nanoscale coaxial lasers. *Nature* **482**, 204–207 (2012).
This work shows a nanolaser with spontaneous emission coupling factor close to unity.
59. Hayenga, W. E. et al. Second-order coherence properties of metallic nanolasers. *Optica* **3**, 1187–1193 (2016).
60. Ma, R. M., Yin, X. B., Oulton, R. F., Sorger, V. J. & Zhang, X. Multiplexed and electrically modulated plasmon laser circuit. *Nano Lett.* **12**, 5396–5402 (2012).
This work demonstrates a waveguide-embedded plasmonic nanolaser.
61. Chou, Y.-H. et al. Ultracompact pseudowedge plasmonic lasers and laser arrays. *Nano Lett.* **18**, 747–753 (2018).
62. Symonds, C. et al. Confined Tamm plasmon lasers. *Nano Lett.* **13**, 3179–3184 (2013).
63. Lheureux, G. Polarization-controlled confined Tamm plasmon lasers. *ACS Photonics* **2**, 842–848 (2015).
64. Shen, K. C. et al. Deep-ultraviolet hyperbolic metacavity laser. *Adv. Mater.* **30**, 1706918 (2018).
65. Wang, X.-Y., Chen, H.-Z., Wang, S., Zhang, S. & Ma, R.-M. Chiral-reversing vortex radiation from a single emitter by eigenstates phase locking. https://arXiv.org/1707.01055 (2017).
66. Zhou, W. et al. Lasing action in strongly coupled plasmonic nanocavity arrays. *Nat. Nanotech.* **8**, 506–511 (2013).
This work reports a plasmonic array laser with a configuration of metal particles.
67. Van Beijnum, F. et al. Surface plasmon lasing observed in metal hole arrays. *Phys. Rev. Lett.* **110**, 206802 (2013).
This work reports a plasmonic array laser with a configuration of metal holes.
68. Yang, A. K. et al. Real-time tunable lasing from plasmonic nanocavity arrays. *Nat. Commun.* **6**, 6939 (2015).
69. Schokker, A. H. & Koenderink, A. F. Lasing in quasi-periodic and aperiodic plasmon lattices. *Optica* **3**, 686–693 (2016).
70. Tenner, V. T., de Dood, M. J. A. & van Exter, M. P. Measurement of the phase and intensity profile of surface plasmon laser emission. *ACS Photonics* **3**, 942–946 (2016).
71. Wang, D. et al. Band-edge engineering for controlled multi-modal nanolasing in plasmonic superlattices. *Nat. Nanotech.* **12**, 889–894 (2017).
72. Wang, D. et al. Stretchable nanolasing from hybrid quadupole plasmons. *Nano Lett.* **18**, 4549–4555 (2018).
73. Kim, H., Lee, W.-J., Farrell, A. C., Balgarkashi, A. & Huffaker, D. L. Telecom-wavelength bottom-up nanobeam lasers on silicon-on-insulator. *Nano Lett.* **17**, 5244–5250 (2017).
74. Ha, S. T. Directional lasing in resonant semiconductor nanoantenna arrays. *Nat. Nanotech.* https://doi.org/10.1038/s41565-018-0245-5 (2018).
This work demonstrates a dielectric nanoparticle array laser.
75. Yokoyama, H. & Brorson, S. Rate equation analysis of microcavity lasers. *J. Appl. Phys.* **66**, 4801–4805 (1989).
76. Björk, G. & Yamamoto, Y. Analysis of semiconductor microcavity lasers using rate equations. *IEEE J. Quant. Electron.* **27**, 2386–2396 (1991).
77. Yokoyama, H. et al. Controlling spontaneous emission and threshold-less laser oscillation with optical microcavities. *Opt. Quant. Electron.* **24**, S245–S272 (1992).
78. Purcell, E. M. Spontaneous emission probabilities at radio frequencies. *Phys. Rev.* **69**, 681 (1946).
79. van Exter, M. P., Nienhuis, G. & Woerdman, J. P. Two simple expressions for the spontaneous emission factor β. *Phys. Rev. A* **54**, 3553 (1996).
80. Altug, H., Englund, D. & Vuckovic, J. Ultrafast photonic crystal nanocavity laser. *Nat. Phys.* **2**, 484–488 (2006).
81. Lau, E. K., Lakhani, A., Tucker, R. S. & Wu, M. C. Enhanced modulation bandwidth of nanocavity light emitting devices. *Opt. Express* **17**, 7790 (2009).
82. Ni, C.-Y. A. & Chuang, S. L. Theory of high-speed nanolasers and nanoLEDs. *Opt. Express* **20**, 16450 (2012).
83. Pan, S. H., Deka, S. S., Amili, A. E., Gu, Q. & Fainman, Y. Nanolasers: second-order intensity correlation, direct modulation and electromagnetic isolation in array architectures. *Progr. Quant. Electron.* **59**, 1–18 (2018).
84. Wang, S., Chen, H.-Z. & Ma, R.-M. High performance plasmonic nanolasers with external quantum efficiency exceed 10%. *Nano Lett.* https://doi.org/10.1021/acs.nanolett.8b03890 (2018).
85. Sauvan, C., Hugonin, J. P., Maksymov, I. S. & Lalanne, P. Theory of the spontaneous optical emission of nanosize photonic and plasmon resonators. *Phys. Rev. Lett.* **110**, 237401 (2013).
86. Cisco. *The Zettabyte Era: Trends and Analysis* (Cisco, 2017); https://www.cisco.com/c/en/us/solutions/collateral/service-provider/visual-networking-index-vni/vni-hyperconnectivity-wp.html
87. Tucker, R. S. Green optical communications part II: energy limitations in networks. *IEEE J. Sel. Top. Quant. Electron.* **17**, 261–274 (2011).
88. Tatum, J. A. et al. VCSEL-based interconnects for current and future data centers. *J. Lightw. Technol.* **33**, 727–732 (2015).
89. Miller, D. A. B. Device requirements for optical interconnects to silicon chips. *Proc. IEEE* **97**, 1166–1185 (2009).
90. Khurgin, J. B. & Sun, G. Comparative analysis of spasers, vertical-cavity surface-emitting lasers and surface-plasmonemitting diodes. *Nat. Photon* **8**, 468–473 (2014).
91. Strologas, J. & Hess, K. Diffusion capacitance and laser diodes. *IEEE Trans. Electron Devices* **51**, 506–509 (2004).
92. Agrawal, G. P. *Fiber-optic Communication Systems*. 3rd edition (Wiley, New York, 2002).
93. Coldren, L. A. *Diode Lasers and Photonic Integrated Circuits*. 2nd edition (Wiley, New York, 2012).
94. Kim, M.-K., Lakhani, A. M. & Wu, M. C. Efficient waveguide-coupling of metal-clad nanolaser cavities. *Opt. Express* **19**, 23504–23512 (2011).

95. Dolores-Calzadilla, V. et al. Waveguide-coupled nanopillar metal-cavity light-emitting diodes on silicon. *Nat. Commun.* **8**, 14323 (2017).
96. Homola, J. *Surface Plasmon Resonance Based Sensors* (Springer, Berlin, 2006).
97. Zhu, W. et al. Surface plasmon polariton laser based on a metallic trench Fabry–Pérot resonator. *Sci. Adv.* **3**, e1700909 (2017).
98. Gather, M. C. & Yun, S. H. Single-cell biological lasers. *Nat. Photon.* **5**, 406–410 (2011).
99. Fan, X. & Yun, S. H. The potential of optofluidic biolasers. *Nat. Methods* **11**, 141–147 (2014).
100. Humar, M. & Yun, S. H. Intracellular microlasers. *Nat. Photon.* **9**, 572–576 (2015).
101. McGloin, D. Cellular lasers. *Nat. Photon.* **9**, 559–560 (2015).
102. Schubert, M. Lasing within live cells containing intracellular optical microresonators for barcode-type cell tagging and tracking. *Nano Lett.* **15**, 5647–5652 (2015).
103. Chen, Y.-C., Chen, Q. & Fan, X. Lasing in blood. *Optica* **3**, 809 (2016).
104. Chen, Y.-C. et al. Laser-emission imaging of nuclear biomarkers for high-contrast cancer screening and immunodiagnosis. *Nat. Biomed. Eng.* **1**, 724–735 (2017).
105. Martino, N. et al. Micron-sized laser particles for massively multiplexed cellular labelling and tracking. In *Proc. CLEO* JTh5C.6 (OSA, 2018).
106. Cho, S., Humar, M., Martino, N. & Yun, S. H. Laser particle stimulated emission microscopy. *Phys. Rev. Lett.* **117**, 193902 (2016).
107. Liu, X. W. et al. Fluorescent nanowire ring illumination for wide-field far-field subdiffraction imaging. *Phys. Rev. Lett.* **118**, 076101 (2017).
108. Allen, L., Beijersbergen, M. W., Spreeuw, R. J. C. & Woerdman, J. P. Orbital angular-momentum of light and the transformation of Laguerre–Gaussian laser modes. *Phys. Rev. A* **45**, 8185 (1992).
109. Yao, A. M. & Padgett, M. J. Orbital angular momentum: origins, behavior and applications. *Adv. Opt. Photonics* **3**, 161 (2011).
110. Miao, P. et al. Orbital angular momentum microlaser. *Science* **353**, 464 (2016).
111. Wang, X.-Y., Chen, H.-Z., Li, Y., Li, B. & Ma, R.-M. Microscale vortex laser with controlled topological charge. *Chin. Phys. B* **25**, 124211 (2016).
112. Zhen, B. et al. Topological nature of optical bound states in the continuum. *Phys. Rev. Lett.* **113**, 257401 (2014).
113. Kodigala, A. et al. Lasing action from photonic bound states in continuum. *Nature* **541**, 196–199 (2017).
114. Bahari, B. et al. Nonreciprocal lasing in topological cavities of arbitrary geometries. *Science* **358**, 636–640 (2017).
115. Bandres, M. A. et al. Topological insulator laser: experiments. *Science* **356**, eaar4005 (2018).
116. Zhao, H. et al. Topological hybrid silicon microlasers. *Nat. Commun.* **9**, 981 (2018).
117. Parto, M. et al. Edge-mode lasing in 1D topological active arrays. *Phys. Rev. Lett.* **120**, 113901 (2018).
118. Wu, L.-H. & Hu, X. Scheme for achieving a topological photonic crystal by using dielectric material. *Phys. Rev. Lett.* **114**, 223901 (2015).
119. Zheludev, N. I., Prosvirnin, S. L., Papasimakis, N. & Fedotov, V. A. Lasing spaser. *Nat. Photon.* **2**, 351–354 (2008).

Acknowledgements

This work was supported by the National Natural Science Foundation of China (grant nos. 11574012, 11774014, 61521004), the Youth 1000 Talents Plan Fund, UK Engineering and Physical Sciences Research council (EP/M013812/1), the Leverhulme Trust (RPG-2016-064) and the EU's Marie Skłodowska-Curie Actions (PIRG08-GA-2010-277080).

Competing interests

The authors declare no competing interests.

Additional information

Reprints and permissions information is available at www.nature.com/reprints.

Correspondence should be addressed to R.-M.M.

Publisher's note: Springer Nature remains neutral with regard to jurisdictional claims in published maps and institutional affiliations.